

# RSC Advances



This is an *Accepted Manuscript*, which has been through the Royal Society of Chemistry peer review process and has been accepted for publication.

*Accepted Manuscripts* are published online shortly after acceptance, before technical editing, formatting and proof reading. Using this free service, authors can make their results available to the community, in citable form, before we publish the edited article. This *Accepted Manuscript* will be replaced by the edited, formatted and paginated article as soon as this is available.

You can find more information about *Accepted Manuscripts* in the [Information for Authors](#).

Please note that technical editing may introduce minor changes to the text and/or graphics, which may alter content. The journal's standard [Terms & Conditions](#) and the [Ethical guidelines](#) still apply. In no event shall the Royal Society of Chemistry be held responsible for any errors or omissions in this *Accepted Manuscript* or any consequences arising from the use of any information it contains.

# Single-Step Label-Free Hepatitis B Virus Detection by Piezoelectric Biosensor

Nicoletta Giambianco<sup>\*a</sup>, Sabrina Conoci<sup>b\*</sup>, Dario Russo<sup>c</sup> and Giovanni Marletta<sup>a</sup>

<sup>a</sup> Laboratory for Molecular Surfaces and Nanotechnology (LAMSUN), Department of Chemical Sciences, University of Catania and CSGI, 95125 Catania, Italy.

<sup>b</sup> STMicroelectronics, Stradale Primosole 50, 95121 Catania, Italy.

<sup>c</sup> Clonit Srl, Via Bernardo Quaranta 57 20139 Milano MI, Italy

Received (in XXX, XXX) Xth XXXXXXXXX 20XX, Accepted Xth XXXXXXXXX 20XX

DOI: 10.1039/b000000x

In this paper we describe a single step and label free method to selectively detect HBV genome based on hybridization with simple linear ssDNA probes immobilized on Au surfaces of a QCM resonator. It has been proved that selective sensing ability is obtained for large DNA target, constituted by HBV clone of 7Kbps through a proper optimization of the probe density. Actually, with a probe density of  $\sim 4.0 \times 10^{12}$  molecules/cm<sup>2</sup> we were able to detect fmol/cm<sup>2</sup> of HBV target, without using any amplification steps or labelling method. The results presented herein pave the way to the development of an easy to use and portable PoC sensors device for direct and fast HBV detection.

## Introduction

The development of nucleic acids biosensors has received increasing attention over the last decade, due to the importance of gene analysis<sup>1</sup> in clinical diagnostics and forensic studies<sup>2</sup>. In this context, most of the consolidated nucleic acids detection methods are time consuming and expensive. Consequently, there is a high demand for accurate biosensors with rapid detection systems in a portable Point-of-Care (PoC) format.

Particularly, for Hepatitis B virus (HBV) detection, there is huge request to detect and monitor at early stage of infection since it is one of the major health problems worldwide leading to chronic hepatitis, cirrhosis and primarily liver cancer<sup>3-4</sup>.

The Hepatitis B virus (HBV) is a mostly double-stranded DNA virus in the Hepadnaviridae family. The HBV virion genome is circular and approximately 3.2 kb in size and consists of DNA that is mostly double stranded. It has compact organization, with four overlapping reading frames running in one direction and no noncoding regions<sup>5</sup>.

Currently, the most commonly used clinical diagnostic methods for HBV detection are based on immunoassay and polymerase chain reaction (PCR). Immunoassays present a good selectivity and achieve 100% accuracy, but they do not provide quantitative results and the detection is limited by serological response<sup>6</sup>. On the other hands, PCR, that is traditionally the clinical standard technique to quantitatively identify HBV infection, requires

complex and high cost instrumentation<sup>7</sup>.

DNA biosensors based on nucleic acids hybridization are currently under intense investigation owing to their increasing importance in the diagnosis of diseases, with low cost and low power requirements<sup>8-10</sup>.

Among the methods developed for hybridization analysis, the most attractive ones for portable PoC devices are those based on electronic detection since they offer the advantages to be easily integrated with microelectronics in miniaturized chip-based format<sup>11,12</sup>. Recently, increasing attention has been paid to the development of quartz crystal microbalance (QCM) biosensors due to their many merits such as compact size, high mass sensitivity, easiness to be properly functionalised in view of good specificity, low cost, label-free detection and rapid response<sup>13-16</sup>. Indeed, QCM detection methods require device architectures implying to immobilize specific DNA probes on Au surfaces. However, such methodologies require the control of the accessibility, in order to enable the full accessibility of the detection sites on the probe. In fact, the immobilized probe molecules may suffer a significant reduction of the appropriate exposure of the recognizing sites, when compared to the efficiency of probe-target recognition in solution. Despite extensive investigations at this regard<sup>17-23</sup> only a limited number of studies have been addressed to the detection of large DNA target without amplification<sup>24,25</sup>.

Accordingly, the performances of QCM-based biosensor devices (i.e. specificity, sensitivity and reproducibility) are supposed to strictly depend on the control of both homogeneity and structural features of the immobilized DNA probes, respectively involving packing density and molecular conformation<sup>26-29</sup>. One of the

<sup>a</sup>Department of Chemical Sciences, University of Catania, 95125 Catania, Italy. E-mail: [n.giambianco@unict.it](mailto:n.giambianco@unict.it)

<sup>b</sup>STMicroelectronics, Stradale Primosole 50, 95121 Catania, Italy. E-mail: [sabrina.conoci@st.com](mailto:sabrina.conoci@st.com)

approach to improve biosensor ability and overcome the limitations in the case of large DNA target recognition, is therefore to design devices based on complex nanoarchitectures of DNA probes<sup>30,31</sup> involving multistep surface chemistry<sup>32</sup>.

Again, this would represent a serious drawback for an industrial scale-up of the process.

In order to face the problems described above, in this paper we describe a single step and label free method to perform gene analysis, showing its application, as a model system, to the selective detection of HBV genome based on hybridization with simple linear ssDNA probes immobilized on Au surfaces of QCM resonator. In particular, it is shown that fast and selective sensing ability is obtained for large DNA target, constituted by HBV clone of 7Kbps through a proper optimization of the probe density. The results presented herein are very promising for the development of an easy-to-use, portable PoC sensors device for direct and fast HBV detection.

## Experimental

### 2.1 Materials and methods

Thiolated oligonucleotides probes HBS-F (henceforth indicated as P1) and HBS-R (henceforth indicated as P2) (20, 21 nts) were purchased from Eurofins MWG Operon and were prepared with concentration range 0.08  $\mu\text{M}$  - 38.8 $\mu\text{M}$  in ultrapure water (DNase and RNase-free, Gibco). The ultrapure water osmolality is certified to be 1.0 mOsm/kg with pH 6.0.

Stock solutions of Hepatitis B virus (HBV) clone complete genome (T-clone) (Ref. 05960467, consisting in HBV genome 3.2 Kbps and a plasmid PBR322 vector 3.8Kbps) in TE (Tris 10mM, EDTA 1mM, pH=8), R-clone (Ref. RT 50, consisting of Factor V of Leiden of 6,062 Kbps) in TE (Tris 10mM, EDTA 1mM, pH=8) were provided by Clonit. These were diluted at concentration of 370 pg in ultrapure water (pH =8.1 $\pm$ 0.2). Both these solutions (T-clone and R-clone) were denatured at 95 degrees for 5' and immediately immersed in ice bath before use.

The recognition site on hepatitis B-virus for ssDNA probe sequences P1 and P2 are located at the core protein coded for by gene C (HBcAg) at nucleotide position 1 (P2) and 181 (P1), respectively<sup>33</sup>.

**Table 1.** Reports the sequence, size and molecular weight (MW) of thiolated DNA P1 and P2 probes (complementary to T-Clone) and genomic target (R and T-clone).

Name	Sequences (5' to 3')	Size	MW (g/mol)
P1	HBS-F CACATCAGGATTCCTAGGAGG	21 nts	6570
P2	HBS-R GGTGAGTGATTGGAGGTTGG	20 nts	6519
T-clone	HBV	7000 bps	4.6 x10 <sup>6</sup>
R-clone	Factor V of Leiden	6062 bps	4.1x10 <sup>6</sup>

### 2.2 Instrumentation

#### 2.2.1 Quartz crystal microbalance with dissipation monitoring (QCM-D)

QCM-D measurements were carried out with a Q-Sense E1 Instrument. The gold-coated QCM crystals (QSX 301) consisting of a 100 nm layer of gold with 5 nm chromium adhesion layer were purchased from Q-Sense, Inc. The substrates were cleaned by treatment of UV-O<sub>3</sub> for 20 minutes, rinsed with Millipore water and dried with N<sub>2</sub> flow. Specifically, the QCM-D experiments were carried out in two steps as follows:

a) Probe immobilization study: it started by flowing ultrapure water solutions (H<sub>2</sub>O), followed by thiolated ssDNA probes (P1 and P2) solutions at various concentrations (38.8 $\mu\text{M}$ , 7.7 $\mu\text{M}$ , 0.8  $\mu\text{M}$  and 0.08 $\mu\text{M}$ ) with nuclease free water and monitoring the related frequency and dissipation changes. After that, rinsing steps are carried out to remove the excess of probe not linked to the surface.

b) Target Recognition: it started by flowing at first solution of R-clone, at a concentration of 370 pg, followed by a rinsing step, and by the subsequent injection of the specific genome target (T-clone) with a final rinsing step. Ultrapure water was used during the probe immobilization and target hybridization steps.

All measurements were performed at temperature of 25°C. At the frequency overtones, 15 MHz, 25 MHz, 35 MHz, 45 MHz, 55 MHz and 65 MHz, the  $\Delta f$  shifts and  $\Delta D$  were obtained with an accuracy of  $\pm 0.2$  Hz and  $\pm 0.2 \times 10^{-6}$  respectively. Frequency ( $\Delta f$ ) and dissipation ( $\Delta D$ ) shifts were measured with respect to a baseline obtained in ultrapure water.

#### 2.2.2 Atomic force microscopy (AFM)

Atomic force microscopy (AFM) was employed to measure the surface morphology at nanometer scale with Multi-mode/Nanoscope IIIA Atomic Force Microscope (AFM) (VEECO, USA) in tapping mode in liquid with a standard silicon tip (40-75 kHz frequency resonance and force constant 0.58 N/m). The ex-situ samples were prepared by incubating 350  $\mu\text{l}$  of the ssDNA probe solutions (P1) at concentration 0.8 $\mu\text{M}$  on gold substrates for 30 minutes, then rinsing with 350  $\mu\text{l}$  and gently drying with N<sub>2</sub> flow. After the ssDNA incubation step, the samples were then incubated with 350  $\mu\text{l}$  R-clone or T-clone solution and imaged by AFM in H<sub>2</sub>O. Data were acquired on square frames having edges 500 nm. The scan rate was 1.0 Hz. Images were recorded using both height channels with 512 x 512 measurement points (pixels). Only flattening was employed to remove the background slope processed images. Measurements were made twice on different zones of each sample. The root-mean-square (RMS) surface roughness was used to quantify variations in surface elevation over different scans area.

## Results and discussion

### 3.1. Probe Anchoring Study

#### 3.1.1 Determination of DNA probe density using QCM-D

The immobilization of two thiol-labeled ssDNA oligonucleotides P1 and P2, respectively, onto Au surfaces, have been studied in situ by means of QCM with dissipation monitoring (QCM-D).

Fig 1 reports the measured real time acoustic QCM-D curves in a

concentration range of 0.8–38.8  $\mu\text{M}$  for the probe P1 (Fig. 1a) and probe P2 (Fig. 1b). In this range, small but detectable amounts of adsorbed probes are found; while below the concentration of 0.8  $\mu\text{M}$  (i.e., 0.08  $\mu\text{M}$ ) no significant adsorption has been found.

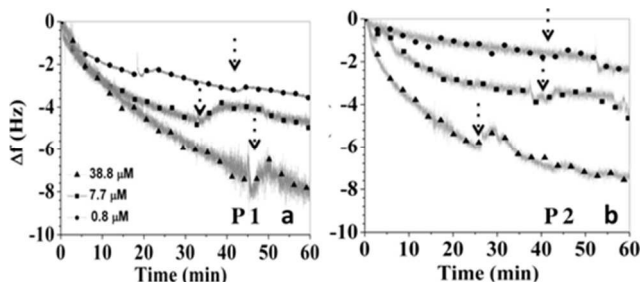


**Figure 1.** Real time acoustic QCM-D curves (15 MHz). Frequency changes due to the adsorption of thiolated ssDNA probe P1 (a) and probe P2 (b) on gold are reported for solution concentrations of 38.8  $\mu\text{M}$  (triangles), 7.7  $\mu\text{M}$  (square), 0.8  $\mu\text{M}$  (circle). Each sample addition is followed by the rinsing step indicated with arrows ( $\text{H}_2\text{O}$ ).

According to Fig. 1, three kinetic steps can be identified: (i) probe adsorption ( $\Delta f < 0$ ) during the surface exposure at the probe solutions; (ii) small probe desorption ( $\Delta f > 0$ ) during the rinsing step; (iii) a further step, after rinsing, where the frequency decrease again ( $\Delta f < 0$ ). According to literature<sup>34</sup>, we propose that the ssDNA molecules are anchored to the gold, via the thiol group, in a standing-up position. The further frequency decreasing after the rinsing step (iii) can be attributed to the adsorption of a water shell around the DNA molecules, enabling the ssDNA molecules to extend farther out into the water according to literature<sup>34</sup>.

Table 2 reports the averaged values measured for frequency and dissipation changes upon P1 and P2 probe adsorption. Since the measured energy dissipation  $\Delta D$  is low, the Sauerbrey frequency-mass relationship can be used to calculate the amount of anchored probe<sup>35</sup>. According to Sauerbrey, the relationship between frequency change ( $\Delta f$ ) and mass adsorbed ( $\Delta m$ ) is given by  $\Delta m = -\Delta f \times C_n$ , where  $n$  is the harmonic number and  $C$  is an experimental constant characteristic of the employed sensor and equal to  $\sim -17.7 \text{ ng}/(\text{cm}^2\text{Hz})$  for a 5-MHz crystal. The measured averaged  $\Delta f$  values for the three solution concentrations of probe P1, after the first hour of adsorption, were  $-7.5 \pm 0.3 \text{ Hz}$  (38.8  $\mu\text{M}$ ),  $-5.0 \pm 0.4 \text{ Hz}$  (7.7  $\mu\text{M}$ ) and  $-2.8 \pm 0.2 \text{ Hz}$  (0.8  $\mu\text{M}$ ), respectively corresponding to about  $132.75 \pm 5.3 \text{ ng}/\text{cm}^2$ ,  $88.5 \pm 7.8 \text{ ng}/\text{cm}^2$  and  $49.6 \pm 3.5 \text{ ng}/\text{cm}^2$  of adsorbed mass. According to that, the respective ssDNA probe surface densities can be estimated to be  $1.2 \pm 0.6 \times 10^{13} \text{ molecule}/\text{cm}^2$  (from 38.8  $\mu\text{M}$  solution),  $8.2 \pm 0.5 \times 10^{12} \text{ molecule}/\text{cm}^2$  (from 7.7  $\mu\text{M}$ ) and  $4.6 \pm 0.3 \times 10^{12} \text{ molecule}/\text{cm}^2$  (from 0.8  $\mu\text{M}$ ) respectively. Similar results for the adsorption process with slightly lower surface density values were measured for the P2 ssDNA probe (Fig. 1b and Table 2b). The obtained surface density values are in good agreement with the literature for similar anchoring studies<sup>18</sup>.

**Table 2.** Frequency ( $\Delta f$ ), dissipation shifts ( $\Delta D$ ), number of molecules/ $\text{cm}^2$  and neighbour distance ( $d$ ) of P1 (2a) and P2 (2b) probes adsorbed on gold.

a) P1 probe

[P1] conc. ( $\mu\text{M}$ )	$\Delta D (10^{-6})$	$\Delta f (\text{Hz})$	Number of molecules/ $\text{cm}^2 (10^{12})$	$d (\text{nm})$
38.8	$2.5 \pm 0.3$	$-7.5 \pm 0.3$	$12.0 \pm 0.6$	$2.9 \pm 0.2$
7.7	$1.9 \pm 0.2$	$-5.0 \pm 0.4$	$8.2 \pm 0.5$	$3.5 \pm 0.1$
0.8	$0.6 \pm 0.2$	$-2.8 \pm 0.2$	$4.6 \pm 0.3$	$4.7 \pm 0.1$

b) P2 probe

[P2] Conc. ( $\mu\text{M}$ )	$\Delta D (10^{-6})$	$\Delta f (\text{Hz})$	Number of molecules/ $\text{cm}^2 (10^{12})$	$d (\text{nm})$
38.8	$2.8 \pm 0.3$	$-6.2 \pm 0.3$	$10.0 \pm 0.6$	$3.2 \pm 0.2$
7.7	$1.5 \pm 0.2$	$-4.0 \pm 0.4$	$6.4 \pm 0.5$	$3.9 \pm 0.1$
0.8	$0.5 \pm 0.2$	$-2.3 \pm 0.2$	$3.7 \pm 0.3$	$5.2 \pm 0.1$

### 3.1.2 Binding energy from adsorption data

The bonding between the ssDNA molecules and gold surface can be understood by deriving the binding energy from the equilibration adsorption data (reached after 1h). In particular, the equilibrium data at the three surface densities here studied for P1 and P2 probes perfectly fit a simple Langmuir model (Fig. 2 for P1 and Fig. SI2 for P2).

The equilibrium-binding constant of the ssDNA probes on gold ( $K_e$ ) can be calculated by equation 1,

$$(d\Gamma(t))/dt = K_e C(1-(\Gamma(t))/\Gamma_{\text{max}}) \quad \text{Eq.1}$$

where  $K_e = k_{\text{ads}}/k_{\text{des}}$ ,  $d\Gamma(t)$  is the time-dependent surface density for the adsorbed molecules ( $\text{N molecules}/\text{cm}^2$ ),  $\Gamma_{\text{max}}$  is the maximum possible coverage and  $C$  is the ssDNA probe concentration in solution.

The fitting of the experimental data by equation 1, yields the following values for P1 and P2 equilibrium constants:  $K_e (\text{P1}) = 6.0 \pm 1.0 \times 10^5 \text{ M}^{-1}$  and  $K_e (\text{P2}) = 4.0 \pm 0.5 \times 10^5 \text{ M}^{-1}$ .

The knowledge of the  $K_e$  values, hence, allows the derivation of the free energies of adsorption of thiolated ssDNA probes P1 and P2 on gold, according to the well known relation  $\Delta G = -RT \ln K_e$ , where  $K_e = k_{\text{ads}}/k_{\text{des}}$ . In particular, from the values of  $K_e$  above reported, we obtained  $\Delta G_{\text{ads}}(\text{P1}) = -42.0 \pm 3.6 \text{ kJ mol}^{-1}$  ( $-10.3 \pm 0.9 \text{ kcal mol}^{-1}$ ) and  $\Delta G_{\text{ads}}(\text{P2}) = -43.0 \pm 3.0 \text{ kJ mol}^{-1}$  ( $-10.5 \pm 0.7 \text{ kcal mol}^{-1}$ ). These values are in close agreement with those expected for gold/thiol bond formation ( $-40 \text{ kJ mol}^{-1}$ )<sup>36</sup>. This finding supports the fact that the adsorption process essentially involves covalently bonded species, with a negligible role, if any, of non-specific interactions (i.e., van der Waals, image charge, etc.). Moreover, it has been recently proved that the Au-S bond



formation (isolated molecules) is very fast (8 s)<sup>37</sup> indicating that in our case, after 20 minutes (flowing time of probe surface exposure), all the thiolated probes are covalently bound.

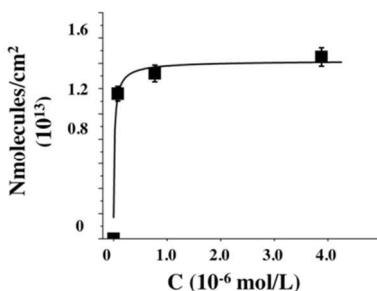


**Figure 2.** Surface coverage (N molecules/cm<sup>2</sup>) versus solution concentration (C) of thiolated ssDNA probe (P1) after 1 hour. The correlation coefficient is R<sup>2</sup> = 0.94.

The data reported in Fig. 2 indicate that adsorption is roughly ranging between  $\sim 3.0 \times 10^{12}$  and  $1.2 \times 10^{13}$  molecules/cm<sup>2</sup>, reaching a plateau value thereafter, in agreement with similar results reported in literature<sup>38,49</sup>.

### 3.1.1 Average nearest neighbour-distance

The average nearest neighbour distance was estimated by the equation  $d = 1/\sigma^{1/2}$ , where  $\sigma$  is the measured probe density, under the assumption that the system consists in an hexagonal close-packed array of thiolated DNA probes. In particular, for probe P1 we have found  $d = 2.9 \pm 0.2$ ,  $d = 3.5 \pm 0.1$  nm and  $4.7 \pm 0.1$  nm, respectively for the experimental densities of  $1.2 \pm 0.6 \times 10^{13}$ ,  $8.2 \pm 0.5 \times 10^{12}$  and  $4.6 \pm 0.3 \times 10^{12}$  molecules/cm<sup>2</sup>. These values correspond to one ssDNA molecule per 9.0 nm<sup>2</sup>, one ssDNA per 13 nm<sup>2</sup> and one ssDNA per 22 nm<sup>2</sup>, respectively. A similar trend, with lower values have been found for P2 ssDNA probe, i.e.,  $d = 3.2 \pm 0.2$  nm,  $d = 3.9 \pm 0.1$  nm and  $d = 5.2 \pm 0.1$  nm for the experimental density of  $1.0 \pm 0.6 \times 10^{13}$  molecules/cm<sup>2</sup>,  $6.4 \pm 0.5 \times 10^{12}$  molecules/cm<sup>2</sup> and  $3.7 \pm 0.5 \times 10^{12}$  molecules/cm<sup>2</sup>. Again, these values correspond to one ssDNA molecule per 10 nm<sup>2</sup>, one ssDNA per 15 nm<sup>2</sup> and one ssDNA molecule per 27 nm<sup>2</sup>, respectively. The above data suggest that the probe sequence may have a small effect on the total adsorbed mass, and, thus, on the chain density.

Also, the possible contribution of conformational and entropic forces, i.e., steric hindrance factors, to the distribution of the ssDNA strands along the gold surface have been analysed. In particular, we have compared the size of the free thiolated ssDNA molecules in solution with the estimated average distance among neighbouring chemisorbed molecules on gold, for the various measured surface densities. The contour lengths of fully stretched ssDNA strands is simply  $L = bN$ , where N is the number of bases in the strand and  $b \cong 0.7$  nm is the distance between adjacent phosphorous atoms<sup>40</sup>. In our case  $L$  (P1) = 14.7 nm for N = 21 nts (P1 strands), and  $L$  (P2) = 14.0 nm for N = 20 nts (P2 strands). On the other hand, the real size of the thiolated

ssDNA P1 strands can be described by means of the persistence length ( $l_p$ ), which, for the studied ssDNA strands is about 6.7 nm at the low ionic strength solutions here employed (i.e., ultrapure water)<sup>41</sup>. In this framework, the ssDNA molecules, under the condition  $l_p < L$ , can be represented as semiflexible coils. In a simple bidimensional model, consisting of hexagonal close-packed arrangement<sup>42</sup>, a distribution of weakly stretched ssDNA brushes<sup>43</sup>, extending towards the solution, is therefore expected, according to well-established literature<sup>44</sup>.

## 3.2 Target Recognition

### 3.2.1 Crowding effect on target recognition

The effect of the ssDNA probes density on the recognition efficiency and selectivity towards genomic DNA targets has been studied with respect to a specific genomic target T-clone and a non-complementary genome R-clone, both at concentration of 370 pg (denaturated at 95°C before hybridization). In the following discussion we focus the attention to the response of P1 probe to the T and R clones, as for P2 very similar effects have been observed.

Fig 3 shows the measured real time hybridization QCM-D curves for the three surface densities cases of P1 probe:  $1.2 \times 10^{13}$  molecules/cm<sup>2</sup>,  $8.2 \times 10^{12}$  molecules/cm<sup>2</sup> and  $4.6 \times 10^{12}$  molecules/cm<sup>2</sup>. It can be noticed that the most efficient hybridization is found for the probe density surfaces of  $4.6 \times 10^{12}$  molecules/cm<sup>2</sup> (the lowest here explored) while the higher surface density samples show an almost negligible hybridization capability. In particular, Fig.3a and b show that the surfaces with highest P1 probe density ( $1.2 \times 10^{13}$  molecules/cm<sup>2</sup> and  $8.2 \times 10^{12}$  molecules/cm<sup>2</sup>) produces a small and completely reversible adsorption for both the T- and R-clones, while for the low density surfaces (i.e., about  $4.6 \times 10^{12}$  molecules/cm<sup>2</sup>, Fig 3c) a strongly selective and irreversible hybridization is found for T-clones, as shown by fig.3d, while the non-specific R-clones shows a negligible adsorption. In other words, the  $4.6 \times 10^{12}$  molecules/cm<sup>2</sup> surface density samples show a dramatic increase in selective adsorption of T clone. Moreover, the low density surfaces retained about 45.0 ng/cm<sup>2</sup> of T-clone mass (see Table 3), roughly corresponding to  $1.2 \times 10^{10}$  molecules/cm<sup>2</sup> and, in turn, to 0.02 pmol/cm<sup>2</sup>. Accordingly, the  $4.6 \times 10^{12}$  molecules/cm<sup>2</sup> density surfaces may, in principle, reveal femtomolar concentrations.

**Figure 3.** QCM-D kinetic curves of non-specific R-clones onto the ssDNA probe (P1), followed by washing with H<sub>2</sub>O and then flowed with specific T-clones and a final rinsing step. The ssDNA P1 probe density are a)  $1.2 \times 10^{13}$  molecules/cm<sup>2</sup>; b)  $8.2 \times 10^{12}$  molecules/cm<sup>2</sup>; c)  $4.6 \times 10^{12}$  molecules/cm<sup>2</sup>. Panel d) reports the clone to probe ratios for R/P1 and T/P1 for all the investigated ssDNA surface densities.

As far as the P2-is concerned, the best surface probe density T-clone recognition resulted the same than for P1 ssDNA species, i.e., about  $4.0 \times 10^{12}$  molecules/cm<sup>2</sup>, yielding a genome T-clone

retained mass of  $42 \text{ ng/cm}^2$ , very close to the one measured for P1 (Fig.SI4).

It should be stressed that in this case non-specific R-clones were not adsorbed at all, indicating that neither recognition nor non-specific adsorption events occurred (see Fig. SI 4).

These findings highlight that the recognition of HBV genome is possible by a single step without requiring any amplification procedure.

**Table 3.** Frequency shifts (Hz) and  $\Delta m$  ( $\text{ng/cm}^2$ ) for nonspecific (R) and specific (T) clone hybridized with P1 probe at different surface density.

Probe P1 $\text{Nmoles/cm}^2$ $10^{12}$	R-clone		T-clone	
	$\Delta f$ (Hz)	$\Delta m$ ( $\text{ng/cm}^2$ )	$\Delta f$ (Hz)	$\Delta m$ ( $\text{ng/cm}^2$ )
$12.0 \pm 0.6$	$-0.5 \pm 0.2$	$8.8 \pm 3.5$	$-0.3 \pm 0.2$	$5.3 \pm 3.5$
$8.2 \pm 0.5$	$-0.5 \pm 0.2$	$8.8 \pm 3.5$	$-0.3 \pm 0.2$	$5.3 \pm 3.5$
$4.6 \pm 0.3$	$-0.4 \pm 0.2$	$7.1 \pm 3.5$	$-2.5 \pm 0.3$	$45 \pm 5.3$

### 3.2.2 Topography measurement by AFM

The recognition step is confirmed by AFM analysis. Fig. 4 shows the pictures obtained for reference gold surfaces with immobilized  $8.2 \times 10^{12}$  and  $4.6 \times 10^{12}$  P1-molecules/ $\text{cm}^2$  (Fig. 4 a,c), respectively. Fig. 4 b,d shows the same surfaces reacted with T-clone solutions. In the case of  $8.2 \times 10^{12}$  P1-molecules/ $\text{cm}^2$  surface, it cannot be seen any T-clone presence (Fig. 4b). On the contrary, the presence of circular HBV can be recognized on  $4.6 \times 10^{12}$  P1-molecules/ $\text{cm}^2$  surface, supporting the occurred hybridization above described. In this case, the obtained results support the grain size analysis, suggesting that the recognition basically involves  $42 \pm 7.0$  nm long T-clone isolated molecules with an average distance between two neighboring HBV of about  $70.0 \pm 8.0$  nm. The number of HBV T-clone counted in the inspected AFM area ( $500 \text{ nm} \times 500 \text{ nm}$ ) is therefore about 30. By considering the P1 probe density ( $4.6 \times 10^{12}$  molecules/ $\text{cm}^2$ ), the theoretical P1/T-Clone ratio in the inspected AFM area is about 400.

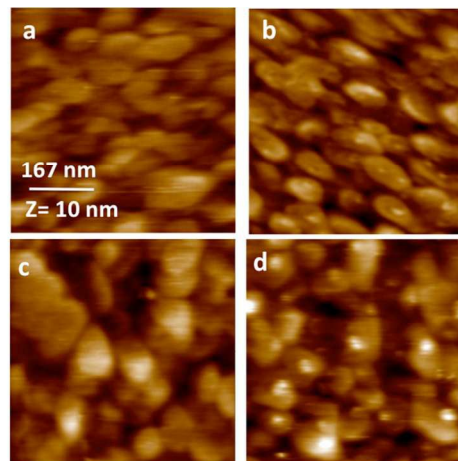


**Figure 4.** Height AFM images of gold surfaces functionalized with thiolated ssDNA from  $7.7 \mu\text{M}$  (a) and  $0.8 \mu\text{M}$  (c) solution; AFM images of the thiolated surfaces exposed to T-clone (b) and (d).

The AFM results found a nice confirmation by comparing them to the data of surface densities for P1 and retained density of T-clone measured by QCM-D. Indeed, by calculating the hybridization HBV:P1 probes ratio, i.e., the retained  $1.2 \times 10^{10}$  molecules/ $\text{cm}^2$  HBV and the  $4.6 \times 10^{12}$  molecules/ $\text{cm}^2$  P1 probe density, a value of about 400:1 is obtained as well.

### 3.2.3 Kinetics of recognition and hybridization of target onto probes

The analysis, according to a simple first-order Langmuir kinetics, of the time-dependent T-clone mass uptake for the three different probe density surfaces provide further hints on the hybridization process<sup>45</sup>:

$$\frac{d\sigma_T}{dt} = k_a C_T (\sigma_P - \sigma_T) - k_d \sigma_T \quad \text{Eq.2}$$

where  $k_a$  and  $k_d$  are the association and desorption rate constants,  $C_T$  is the bulk concentration of HBV target,  $\sigma_T$  is the surface density of hybridized molecules of target,  $\sigma_P$  is the surface probe density. If target is constant (as it is continuously and in excess, this can be integrated to

$$\sigma_T(t) = \sigma_T^{eq} (1 - \exp(-k_{eff} t)) \quad \text{Eq.3}$$

where  $k_{eff} = k_a C_T + k_d$  is the effective rate constant. The characteristic time scale of the reaction is given by  $\tau = 1/k_{eff}$  taking into account an association rate constant,  $k_a$  and a desorption constant,  $k_d$ .

Fig. 5 reports the kinetic curves of mass change ( $\text{ng/cm}^2$ ) vs  $t$  (s) for the two processes: (i) target hybridization ( $\Delta m > 0$ ) during the surface exposure at the target solution; (ii) target excess desorption ( $\Delta m < 0$ ) during the rinsing step.

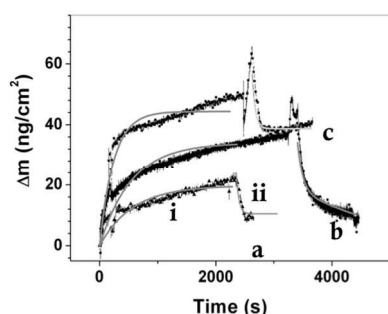


**Figure 5.** Mass uptake curves versus time (*t*) measured by means of QCM-D technique for specific genomic T-clone onto P1-functionalized gold sensors at various probe densities including  $1.2 \times 10^{13}$  molecules/cm<sup>2</sup> (a),  $8.2 \times 10^{12}$  (b) and  $4.6 \times 10^{12}$  (c) molecules/cm<sup>2</sup>.

All the curves of the hybridized target mass vs time can be fitted by equation 3 with  $\Delta m_{max}$  and  $k_{eff}$  are the fitting parameters.

In particular, since  $\tau = 1/k_{eff} = (k_a C_T + K_d)^{-1}$  and  $C_T$  is the same (370 pg) for the three probe densities,  $\tau_a \sim (k_a C_T)^{-1}$  and  $\tau_d \sim k_d^{-1}$ . Accordingly, Table 3 reports the  $\tau_a$  values obtained by the fitting respectively for target hybridization and target excess desorption  $\tau_d$ , at the three different surface densities of P1 probe.

It can be seen, again, that the values of  $\tau_a \sim 210$  s are obtained for the low probe density surfaces, suggesting that for these surfaces the P1 probe molecules are more accessible than at higher probe density, prompting the observed faster and efficient recognition of HBV-clone molecules (T-clones). Moreover, the high  $\tau_d \sim 1/k_d$  values are almost comparable to  $k_a C_T$ , indicating that the surface concentration of bound targets ( $\sigma_T$ ) will be less than initial surface concentration of probes ( $\sigma_P$ ).

**Table 3.**  $\tau$  (s) values for specific HBV (T) clone hybridization/target excess desorption processes with P1 probe at different surface density

Probe P1 N molecules/cm <sup>2</sup> 10 <sup>12</sup>	T-clone	
	$\tau_a$ (s)	$\tau_d$ (s)
12.0 ± 0.6	1601 ± 100	100 ± 20
8.2 ± 0.5	1002 ± 120	80 ± 10
4.6 ± 0.3	217 ± 20	65 ± 8.0

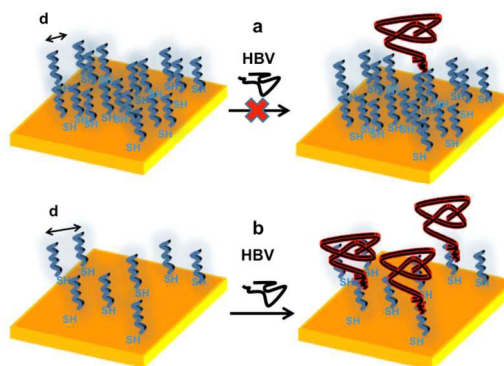
## Conclusions

The data reported above confirm that there is in general a critical probe density threshold to achieve the most effective biomolecules recognition by immobilized probes. In particular, in the case of large HBV virus recognition by means of ssDNA strands as probes, the threshold turns to be about  $4\text{--}5 \times 10^{12}$  probes/cm<sup>2</sup>. Clearly, the density threshold for different probe-target couples depends on the matching of several affinity factors, including the ones controlling the diffusion of the target molecules to the probe hybridization sites, i.e., primarily the

target concentration in solution and the size and conformation of the probes vs. the target to be recognized, as well as the probe-probe spacing. Accordingly, Scheme 1 reports the P1 inter-probe distance respectively for  $1 \times 10^{13}$  molecules/cm<sup>2</sup> and  $4.0 \times 10^{12}$  molecules/cm<sup>2</sup> for the anchored thiolated ssDNA strands. The scheme stresses the difficulty of the target of penetrating the probe layer if the probe densities are too high and the increased facility of clone penetration, turning in a selective recognition, for low-density surfaces.

Additionally, the study revealed an important connection between the effect of ssDNA surface crowding and the kinetic step of HBV hybridization.

Indeed, to our knowledge only few literature reports are dedicated to of the study of the hybridization kinetics of ssDNA towards similar oligonucleotides<sup>18,46-50</sup>, so that the present paper is the first model determining how the ssDNA probe density affects the association and desorption rate with a large genome, in this case the one of HBV virus. In particular, the present study paves the way to a further work aimed to develop quantitative general models for the conception and optimization of DNA chips on new conception, taking profit of a direct and selective recognition process by means of a quartz crystal microbalance sensor, working based on a single step and label free method to selectively detect genome.



**Scheme 1.** Crowding effect in the organization of thiolated ssDNA strands (21 nts) on gold surfaces: a) high probe density surfaces, with hindered HBV hybridization; b) low probe density surfaces, allowing efficient and selective HBV recognition.

The core feature of such a class of devices is clearly based on the controlled hybridization of the target biomolecules with simple linear ssDNA probes suitably immobilized on Au surfaces of the QCM resonator.

To this purpose, the control of surface density, which determines the probe accessibility, is an essential parameter for the final properties of the device and can be quantitatively controlled. Our results show that it is possible to finely control the density and, in turn, the hybridization efficiency also for very large genomes as the one of HBV. This results in a sensitivity of fmol/cm<sup>2</sup>, without the need of any amplification steps or labelling methods. These findings open intriguing prospects towards the fabrication of biosensors able to detect HBV virus in a single-step process.

In summary, the QCM-D biosensors have been shown to exhibit

competitive sensitivity and fast response in detection of HBV virus combined with simple detection protocol and probe immobilization process. The described results, hence, prompt the development of an easy to use single-step and portable PoC sensors device for direct and fast HBV detection.

### Acknowledgments

This work has been funded by MIUR by means of the national Program PON R&C 2007-2013, project “Hyppocrates – Sviluppo di Micro e Nano-Tecnologie e Sistemi Avanzati per la Salute dell’uomo” (PON02 00355) and PRIN 2010-2011 “Metodologie chimiche innovative per biomateriali intelligenti”.

### Notes and references

- 1 J. Wang, *Nucleic Acid Research*, 2000, **28** (16), 3011-3016.
- 2 M. Minunni, S. Tombelli, R. Scielzi, I. Mannelli, M. Mascini, C. Gaudiano, *Anal. Chim. Acta*, 2003, **481**, 55-64.
- 3 C. Trépo, H. L. Y. Chan, A. Lok, *Lancet*, 2014, **384**, 2053–2063.
- 4 R. P. Beasley, *Cancer*, 1988, **61**, 1942-1956.
- 5 Stares, James H. and Ellen G. Stares. 2002. *Viruses and Human Disease*. Academic Press, San Diego, California, 383p.
- 6 A. S. F. Lok, B. J. McMahon, *Hepatology*, 2001, **34**, 1225-1241.
- 7 H. Huang, L. Jin, X. Yang, Q. Song, B. Zou, S. Jiang, L. Sun, G. Zhou, *Biosens. Bioelectron.*, 2013, **42**, 261-266.
- 8 D. Paraskevis, C. Haida, N. Tassopoulos, M. Raptopoulou, D. Tsantoulas, H. Papachristou, V. Sypsa, A. Hatzakis, *J. Virol. Methods*, 2002, **103**, 201-212.
- 9 W. Haasnoot, H. Gerçek, G. Cazemier, M.W. Nielen, *Anal Chim Acta*, 2007, **586**, 312-318.
- 10 D. P. Kalogianni, T. Koraki, T. K. Christopoulos, P. C. Ioannou, *Biosens Bioelectron*, 2006, **21**, 1069-1076.
- 11 T. G. Drummond, M. G. Hill, J. K. Barton, *Nat. Biotechnol.*, 2003, **21**, 1192-1199.
- 12 S. K. Sia, L. J. Kricka, *Lab Chip*, 2008, **8**, 1982 -1983.
- 13 S. Conoci, A. Mascali, F. Pappalardo, *RSC Adv.*, 2014, **4**, 2845–2850.
- 14 C. March, J. J. Manclús, Y. Jiménez, A. Arnau, A. Montoya, *Talanta*, 2009, **78**, 827-833.
- 15 C. Yao, T. Zhu, J. Tang, R. Wu, Q. Chen, M. Chen, B. Zhang, J. Huang, W. Fu, *Biosens. Bioelectron.*, 2008, **23**, 879-885.
- 16 T. Xu, J. Miao, Z. Wang, L. Yu, C. Li, *Sens. Actuators B Chem.*, 2011, **151**, 370-376.
- 17 N. Tuccitto, N. Giambianco, S. Ghosh, V. Spmpinato, P. Labbè, P. Dumy, S. Quici, G. Marletta, E. Defrancq, A. Licciardello, *Langmuir*, 2011, **27** (14), 8595-8599.
- 18 G. Yang, Gao, K. W. Lauren, R. M. Georgiadis, *Nucleic Acids Research*, 2006, **34** (11), 3370–3377.
- 19 T. Strachan, A. P. Read, in *Human Molecular Genetics*. 2nd edition. New York: Wiley-Liss; 2nd edn., 1999, vol. ch. 5, pp. Nucleic acid hybridization assays.
- 20 X. C. Zhou, L. Q. Huang, F. Y. Li Sam, *Biosensor and Bioelectronics*, 2001, **16**, 85-96.
- 21 S. Yamaguchi, T. Shimomura, T. Tatsuma, N. Oyama, *Anal. Chem.*, 1993, **65** (14), 1925–1927
- 22 H. Su, M. Thompson, *Biosens. Bioelectron.*, 1995, 10 (3/4), 329–340.
- 23 F. Caruso, H. Rodda, D.F. Furlong, K. Niikura, Y. Okahata, *Anal. Chem.*, 1997, **69**, 2043–2049.
- 24 C. Yao, T. Zhu, J. Tang, R. Wu, Q. Chen, M. Chen, B. Zhang, J. Huang, W. Fu, *Biosens. Bioelectron.*, 2008, **23**, 879-885.
- 25 X. Zhou, L. Liu, M. Hu, L. Wang, J. Hu, *J Pharm. Biomed. Anal.*, 2002, **27**, 341-345.
- 26 H. Su, C. Sandra, M. Thompson, *Biosens. Bioelectron.*, 1997, **12** (3), 161–173.
- 27 A. W. Peterson, R. J. Heaton, R. M. Georgiadis, *Nucleic Acids Research*, 2001, **24**, 5163-5168.
- 28 Y. Danfeng, K. Junyoung, Y. Fang, E. P. Nielsen, E-K. Sinner, W. Knoll, *Biophysical Journal*, 2005, **88**, 2745–2751.
- 29 D. Irving, P. Gong, R. Levicky, *J. Phys. Chem. B*, 2010, **114** (22), 7631–7640.
- 30 J. Zeng, A. Almadidy, J. Watterson, U. J. Krull, *Sensors and Actuators B*, 2003, **90**, 68–75.
- 31 Y. Ke, S. Lindsay, Y. Chang, Y. Liu, H. Yan, *Science*, 2008, **319**, 180-183.
- 32 C. Lin, Y. Liu, H. Yan, *Biochemistry*, 2009, **48**(8), 1663–1674.
- 33 S. Hernández, M. Venegas, R. A. Villanueva, *Genome Announc.*, 2014, **2**(5), e01075-14.
- 34 J. Mertens, C. Rogero, M.Calleja, D. Ramos, J. A. Martín-Gago, C. Briones, J. Tamayo, *Nature Nanotechnology* 2008, **3**, 301 – 307.
- 35 G. Z. Sauerbrey, *Phys.*, 1959, **155**, 206.
- 36 M. Yang, H.C.M. Chan, *Langmuir*, 1998, **14**, 6121-6129.
- 37 Y. Xue, X. Li, H. Li, W. Zhang, *Nature Communication*, 2015, **5**, 4348-4357.
- 38 A. Singh, S. Snyder, L. Lee, A. P. R. Johnston, F. Caruso, Y. G. Yingling, *Langmuir*, 2010, **26**, 17339–17347.
- 39 Z. F. Gao, J.B. Gao, L. Y. Zhou, Y. Zhang, J. C. Si, H.Q. Luo, N. B. Li, *RCS Advances*, 2013, **3**, 12334-12340.
- 40 S.B. Smith, Y.J. Cui, Bustamante, *Science*, 1996, **271**, 795-799.
- 41 K. Rechendorff, G. Witz, J. Adamcik, G. Dietler, *J. Chem. Phys.*, 2009, **131**, 095103.
- 42 G. Doni, M. D. N. Ngavouka, A. Barducci, P. Parisse, A. De Vita, G. Scoles, L. Casalisce, G. M. Pavan, *Nanoscale*, 2013, **5**, 9988-9993.
- 43 B. Zhao, W.J. Brittain, *Progress in Polymer Science* 2000, Vol. 25, Issue 5, pp. 677–710.
- 44 G. Wu, H. Ji, K. Hansen, T. Thundat, R. Datar, R. Cote, M. F. Hagan, A. K. Chakraborty, A. Mayumdar, *PNAS*, 2001, **98**, 1560-1564.
- 45 D. R. Purvis, D. Pollard-Knight, and P. A. Lowe, in *Commercial Biosensors*, edited by G. Ramsay Wiley-Interscience, New York, 1998, pp.165 – 224.
- 46 B.P.Nelson, T.E. Grimsrud, M.R. Liles, R.M. Goodman, R.M. Corn., *Anal. Chem.*, 2001, **73**, 1-7.
- 47 A.W. Peterson, L.K. Wolf, R.M. Georgiadis, *J. Am. Chem. Soc.* 2002, **124**, 14601-14607.
- 48 A. Vainrub, M.B. Pettitt, *Biopolymers*, 2003, **68**, 265-270.
- 49 P. W. Stevens, J. Sun, D. M. Kelso, *Analytical Biochemistry*, 1999, **276**, 204–214.
- 50 M.F. Hagan, A. K. Chakraborty, *J. Chem. Phys.* 2004, **120**, 4958–4968.